



Synthesis, microstructure and mechanical properties of a bio-inspired Ti-intermetallic multi-layered/SiC_f-reinforced Ti-matrix hybrid composite

Kai Zhu¹, Wenbo Yu^{1,*}, Yann Aman^{2,3}, and Tao Jing^{1,*}

¹ School of Materials Science and Engineering, Tsinghua University, Beijing 100084, China

² Ningbo Institute of Materials Technology and Engineering, CNITECH, Chinese Academy of Sciences, Ningbo 315201, China

³ Laboratory of Chemical Physics, Université Félix Houphouët Boigny, Abidjan, 22 BP 582 Abidjan 22, Côte d'Ivoire

Received: 8 March 2016

Accepted: 13 June 2016

Published online:
20 June 2016

© Springer Science+Business
Media New York 2016

ABSTRACT

In reference to the crack deflection ability of multi-layered keratin and the fibers reinforcement of the dorsal cortex in the turtle shell carapace, a bio-inspired composite of Ti-intermetallic multi-layered/SiC_f-reinforced Ti matrix was successfully fabricated through vacuum hot-pressing sintering using pure titanium foils, pure aluminum foils and continuous SiC ceramic fibers. Our observation reveals that Ti-intermetallic multi-layers were well bonded to each other with the formation of in situ Ti₃Al, TiAl, TiAl₂ and TiAl₃ phases between Ti layers. At the same time, SiC fibers were firmly bonded to the Ti matrix through a circular joining of TiC achieved by the reaction between the deposited coating of C and the Ti matrix. Due to the strengthen effect of continuous-SiC_f-reinforced Ti-matrix part, the tensile and the flexural strengths of the hybrid composite along the longitudinal direction of the fibers were about 636 ± 40 and 889 ± 50 MPa (Ti-intermetallic multi-layered part stressed in tension) or 984 ± 50 MPa (continuous-SiC_f-reinforced Ti-matrix part stressed in tension), respectively. These values were much higher than those obtained from Ti-intermetallic multi-layered composite, corresponding to 404 ± 30 and 462 ± 30 MPa. In addition, the Ti-intermetallic multi-layered composite showed higher fracture toughness value (34.7 ± 1.2 MPa m^{1/2}) than that of continuous-SiC_f-reinforced Ti-matrix composite (24.8 ± 0.1 MPa m^{1/2}). In drop hammer impact test, the hybrid composite exhibited better crack resistance and higher absorb energy when the U notch was in Ti-intermetallic multi-layered side, other than U notch in continuous-SiC_f-reinforced Ti-matrix part. Herein, it is deduced that the hybrid composite combines the crack deflection ability of Ti-intermetallic multi-layered structure and strengthen effect of continuous SiC fibers.

Address correspondence to E-mail: wenboyu@mail.tsinghua.edu.cn; Jintao@mail.tsinghua.edu.cn

Introduction

Due to the special hierarchical organization, structural biological materials feature remarkable mechanical properties, such as high stiffness, high yield strength and impact resistance. Herein, abalone shell, animal bones and mammal teeth have been referenced as models for the purpose of designing bio-inspired synthetic composites with distinctive performances [1–5]. As a typical structure, the turtle shell has carefully been studied to understand the relationship between its complex morphologies and its outstanding protective behavior against the environmental penetration [5–10]. According to these studies, also indicated in Fig. 1a, the turtle shell is a type of functionally graded material, which consists of several different layers, namely keratin layer, cortical layers and an intermediate foam-like cancellous bony layer. Specifically, the outer layer is mainly composed of multi-layered keratin scutes and collagen-fiber-reinforced dorsal cortex, as shown in Fig. 1b. In this way, the multi-layered keratin could deflect the crack propagation with a step structure and the carbonaceous fibers reinforce the dorsal cortex by pulling out and coiling of the fibers, both of which contribute to the shock absorption and help the turtle to defend the assaults from the predators [6], as shown in Fig. 1c. From this point of view, this multi-layered/fiber-reinforced hybrid structure could be treated as a reference for producing advanced engineering materials with desired properties to satisfy some application requirements.

However, until now, only various metal–intermetallic multi-layered materials and continuous-fiber-reinforced metal matrix composites have separately been fabricated and carefully studied, for example Ni–intermetallic multi-layered composite [11, 12], Ti–intermetallic multi-layered composite [13, 14], Cu–Al multi-layered composite [15], Al₂O₃-fiber-reinforced metal matrix composite [16, 17], continuous-SiC_f-reinforced metal matrix composite [6, 18–20] and carbon-fiber-reinforced metal matrix composite. Among these composites, it has been demonstrated that the TiAl-based alloys possess lower density compared to steel- and nickel-based alloys, a higher strength-to-weight ratio compared to aluminum and steel, and excellent creep and corrosion resistance.

Different manufacturing procedures have been adopted for producing Ti–intermetallic multi-layered

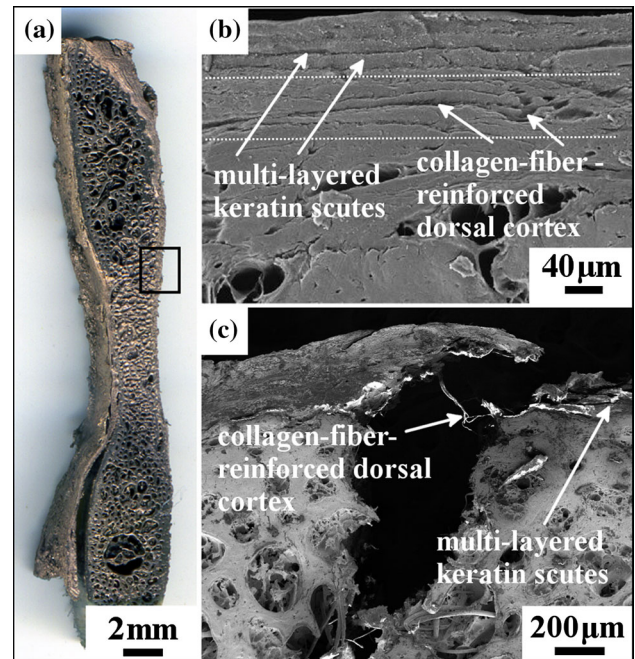


Figure 1 a Cross-sectional structure of the turtle carapace, b enlarged illustration of top of multi-layered keratin scutes and collagen-fiber-reinforced dorsal cortex marked in a, c morphology and propagation of the crack in multi-layered keratin scutes and collagen-fiber-reinforced dorsal cortex after three-point bending test.

composites such as self-propagating high-temperature synthesis (SHS) [11, 13], sintering reaction in air [14], vacuum high-temperature pressing (VHP) [21], hot rolling and hot treatment [22], explosive welding [23] and spark plasma sintering [24]. In these previous works, the microstructure, the interface evolution behavior and the mechanical properties of synthesized composites have been carefully studied. These studies revealed that the coordination deformation behavior between the ductile Ti layers and the highly stiff synthetic intermetallic layers is the main factor leading to their extraordinary properties [12, 25, 26]. As to the continuous SiC fibers with outstanding properties of high strength, high modulus and low density, they have successfully been introduced into the titanium matrix material through vacuum high-temperature pressing (VHP) method [27, 28] and hot isostatic pressing (HIP) method [29]. It has been found that this structural composite possesses an excellent impact resistance, high fatigue resistance and high damage tolerance. The improved properties of toughness and fracture resistance of the composites have been attributed to different mechanisms, such as plastic deformation of matrix materials, fibers

pullout and deflection of cracks at the interface between fibers and matrix materials [30, 31].

Hence, a kind of bio-inspired composite with distinct performance could be obtained if Ti-intermetallic multi-layered composites and continuous-SiC_f-reinforced Ti-matrix composites are manufactured as a whole part. Furthermore, tensile test, flexural test, fracture toughness test and drop hammer impact test were adopted to evaluate this hybrid composite. In addition, these values were also compared with the Ti-intermetallic multi-layered composite and continuous-SiC_f-reinforced Ti-matrix composite.

Experimental procedures

Bio-inspired hybrid structure design

Commercial pure Ti foils (100 μm thick, >99 % in purity) and pure Al foils (20 μm thick, >99 % in purity) were cut into strips with a dimension of 35 mm × 35 mm for later use. And, the initially selected thickness of the foils (Ti:Al = 5:1) was to ensure the complete consumption of the aluminum foils after the reaction sintering process. Chinese fibers (Beijing Institute of Aeronautical Materials, China) with a diameter of 120 μm were chosen as the reinforcement component. These fibers have a tungsten core (16 μm in diameter) and a layer of β-SiC (50 μm thick). In addition, the fibers were coated with a 2-μm layer of carbon by chemical vapor deposition (CVD). In order to improve the bonding quality between the adjacent foil layers, the titanium foils were cleaned in aqueous HF solution (15 %) while the aluminum foils were etched in aqueous NaOH solution (20 %). After the pre-treatment process, those foils were successively rinsed in alcohol and distilled water. Subsequently, all the rinsed foils were dried rapidly in a vacuum drying oven at the

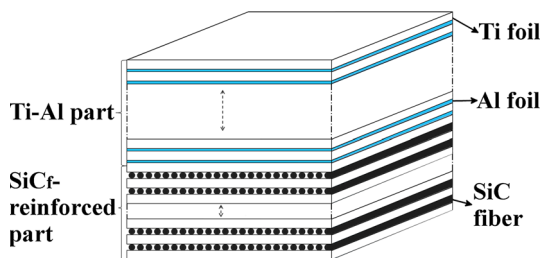


Figure 2 Schematic sequence of stacking of the elemental components.

temperature of 35 °C. Finally, the metallic foils and SiC fibers were stacked according to the schematic order in Fig. 2. It is worth mentioning that all of the fibers were arranged between the two adjacent Ti foils in the same direction.

Sintering procedure

The prepared assembly was moved into a vacuum hot-press furnace (VHP) for producing Ti-intermetallic/SiC_f-reinforced titanium hybrid composite. Typical VHP configuration and processing parameters of the VHP reaction sintering are detailed in Fig. 3.

First, from room temperature to 550 °C, a pressure of 5 MPa was applied to make an adjacent contact among different foils. Secondly, the temperature was maintained at 550 °C for 1 h to achieve a primary combination between the different foils of titanium and aluminum. Afterward, the temperature was increased to 650 °C for initiating and promoting interdiffusion reaction between the dissimilar Ti–Al foils, while the pressure was decreased to 0 MPa for

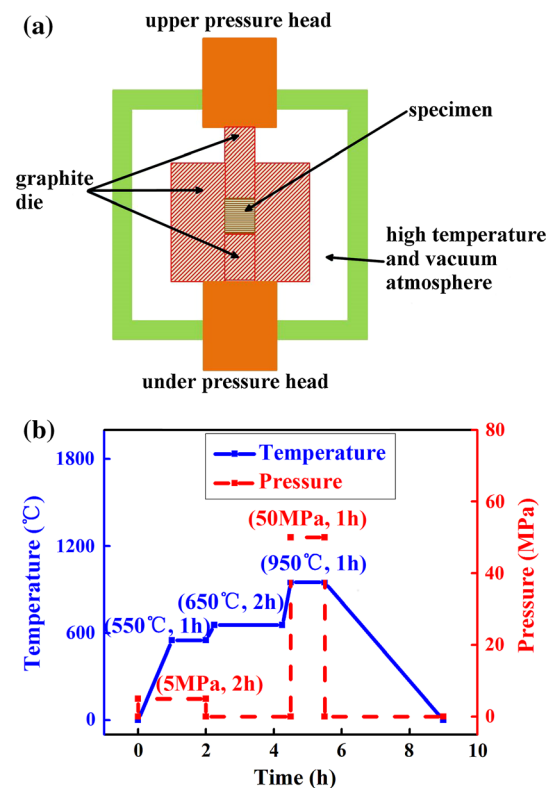


Figure 3 Schematic illustration of the fabrication apparatus and processing parameters: **a** fabrication apparatus and **b** sintering procedure.

avoiding the expulsion of the molten aluminum. This stage lasted 2 h to ensure that all of the aluminum layers were completely consumed into forming Ti–Al compounds. Finally, in order to obtain a tight contact between SiC fibers and Ti matrix, the temperature and pressure were increased to 950 °C and 50 MPa, respectively. In addition, for the purpose of comparison, Ti–Al multi-layered composites and continuous-SiC_f-reinforced Ti-matrix composites were produced by the same procedure.

Materials characterization

The samples were cut from the prepared composite by electro-discharge machining and then mounted in epoxy. Then, the assemblies were ground with silicon carbide and then successively polished with 6, 3, 1 and 0.25 μm diamond suspensions. To avoid the work hardening caused by conventional grinding, a chemomechanical polishing was performed using Al₂O₃ suspension (particle size: 0.04 μm). Phase identification was performed by X-ray diffraction (XRD) using a Bruker (Karlsruhe, Germany) D8 diffractometer with CuK_α radiation. Microstructures and phase compositions were examined by optical

microscopy (OM), scanning electron microscopy (SEM) coupled with energy-dispersive X-ray spectrometry (EDXS).

Mechanical properties measurement

Tensile test and three-point bending test

Uniaxial tensile and three-point bending tests were performed on the hybrid, continuous-SiC_f-reinforced Ti-matrix and Ti-intermetallic multi-layered composites with a universal servo-hydraulic mechanical testing machine at room temperature in air. The hybrid composite specimen was prepared with a volume ratio of 1:1 between the Ti-intermetallic multi-layered part and the continuous-SiC_f-reinforced Ti-matrix part. For the uniaxial tensile test, the selected loading rate was 0.5 mm/min and the specimens were prepared with the dimension of 30 mm × 5 mm × 3 mm, as shown in Fig. 4a. For the three-point bending test, the constant loading rate was 0.2 mm/min. Furthermore, the dimensions of the tested specimens with two different loading patterns are shown in Fig. 4b. The flexural strength σ_f was calculated according to:

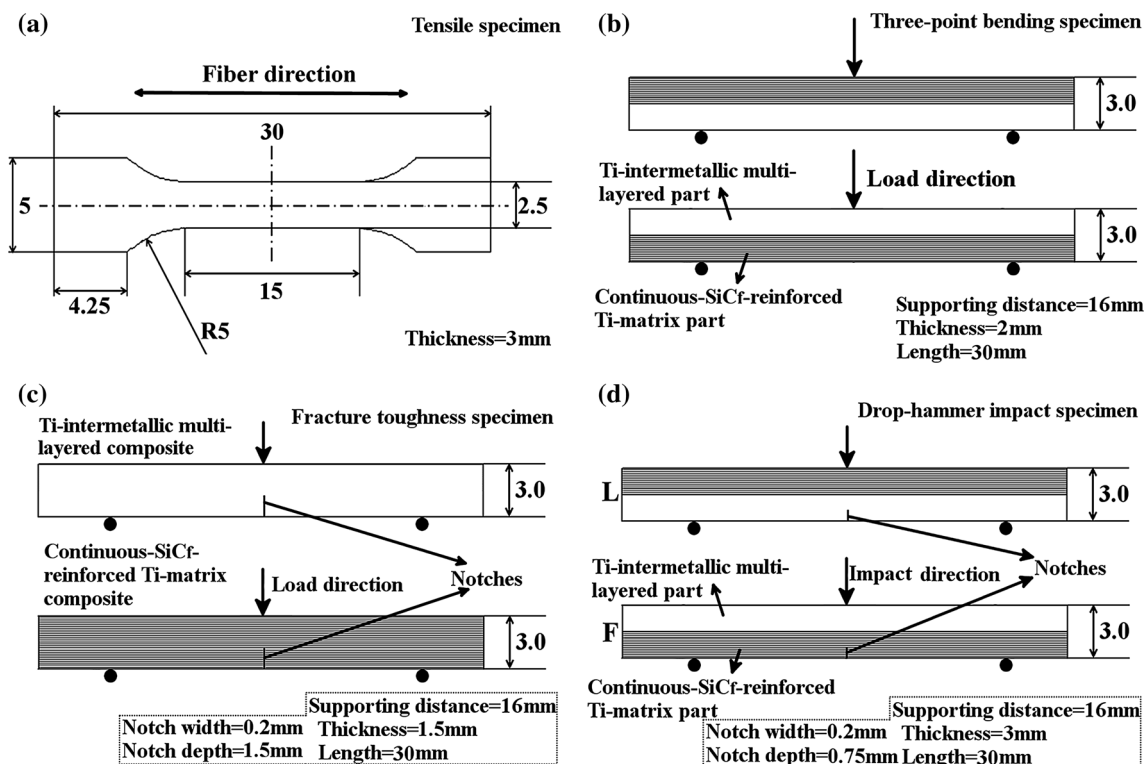


Figure 4 a Outline dimension of the tensile test specimen (unit: mm), b–d are the schematic of the tested specimen in three-point bending test, fracture toughness test and drop hammer impact test.

$$\sigma_f = \frac{3F_{\max}L}{2BW^2} \tag{1}$$

where F_{\max} is the maximum load value of the load–displacement curve of the three-point bended specimens, L is the supporting span of the experiment. B and W are the width and thickness of the specimen, respectively. Each test was repeated six times for each composite in order to evaluate the corresponding mechanical properties.

Fracture toughness test

The fracture toughness of the Ti-intermetallic multi-layered composite and continuous-SiC_f-reinforced Ti-matrix composite was measured by the single-edge pre-cracked beam method. A straight notch was introduced at the center part of the test bar using a 200-μm-wide diamond blade with a notch depth of 0.5 W (the thickness of specimen). To investigate the crack propagation on the notched specimens, the in situ three-point bending test was performed on a servo-hydraulic loading system, which was installed in the vacuum chamber of a scanning electron microscope (Shimadzu Corporation, Japan). During the regular test, a constant loading speed was set as 0.1 mm/min and the dimensions of the tested specimens are shown in Fig. 4c. The fracture toughness was calculated according to ASTM standard E399-90,

$$K_{IC} = \left(\frac{3F_{\max}L}{2BW^2} \sqrt{a} \right) \times f\left(\frac{a}{W}\right) \tag{2}$$

where F_{\max} is the maximum load during the test, L is the supporting distance that we employed during the test, B is the specimen thickness, W is the specimen width (depth), and a is the notch length. In addition, $f(a/W)$ is a geometrical function, which is expressed as:

$$f\left(\frac{a}{W}\right) = 1.964 - 2.837\left(\frac{a}{W}\right) + 13.711\left(\frac{a}{W}\right)^2 - 23.25\left(\frac{a}{W}\right)^3 + 24.129\left(\frac{a}{W}\right)^4 \tag{3}$$

The values of L , B , W and a are taken as 16, 1.5, 3 and 1.5 mm, respectively.

Drop hammer impact test

As the ratio of continuous-SiC_f-reinforced Ti part to Ti-intermetallic multi-layered part is 1:1 in the hybrid

composite, the drop hammer impact test was adopted to evaluate the response of hybrid composites with a U-notch depth of 0.75 mm under impacts. The load (P)–displacement (D) data were recorded by an oscilloscope, and the initial impact energy was set as 10 J. Herein, the dimensions of the two kinds of tested specimens are shown in Fig. 4d.

Results and discussion

Microstructure of the bio-inspired hybrid composite

Figure 5a shows a representative transverse surface of the hybrid composite. It can be seen that the Ti-intermetallic multi-layered part and the continuous-SiC_f-reinforced Ti-matrix part are well bonded to each other. Clearly, as shown in Fig. 5b, in the Ti-intermetallic multi-layered part wherein gray layers (Ti) and white layers (Al or Ti–Al compounds) are alternatively well connected with each other, no interfacial defects and voids are observed. According to Fig. 5c, only 3 connections among 60 fibers are observed, which means that the distribution of the fibers in the Ti matrix is relatively uniform. Furthermore, the SiC_f volume fraction in Ti matrix is about 24 %.

Figure 6 describes the interfacial evolution between Ti and Al foils and the formation of new phases. Typically, EDXS line scans were made along the yellow line to investigate the chemical composition of different layers, as shown in Fig. 6a. The variation of Al content indicates that the layer containing Al (about 30 μm) is much thicker than the original Al foil (20 μm), which means that Al atoms diffused into Ti layers after the high-temperature sintering process. Afterward, EDXS point detects were used to identify the chemical composition of the five spots marked in Fig. 6a. Their chemical compositions are given in Fig. 6c–g and summarized in Table 1. It reveals that the five spots are Ti, Ti₃Al, TiAl, TiAl₂ and TiAl₃, respectively. In detail, from 700 °C and above, previous studies [14, 22, 32, 33] show that TiAl₃ firstly nucleates and forms the continuous layer in Ti–Al intermetallic layers. However, according to the Gibbs energy of formation calculated by Peng et al. [21], the TiAl₃ has a higher free energy of formation than TiAl₂ compounds but lower than TiAl. Herein, the formation of TiAl₃ can be

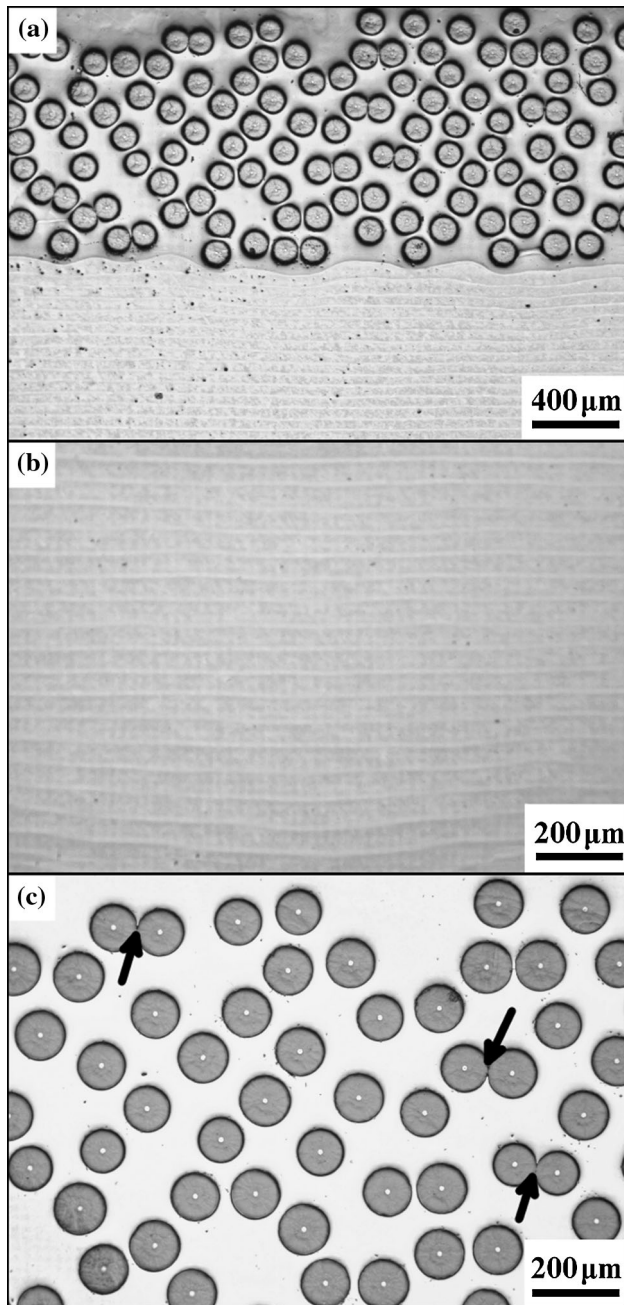


Figure 5 Microstructures of the hybrid composites: **a** transverse micro-photographs of the prepared hybrid composite, **b** Ti-intermetallic multi-layered part and **c** continuous-SiC_f-reinforced Ti-matrix part.

understood from the steps involved in TiAl₂ formation. Furthermore, as reported in [34] the formation of TiAl₂ occurs through a series of solid–liquid and/or solid-state reactions, necessarily involving TiAl as one of the starting phase. In this way, the TiAl₃ phase

was supposed to be formed first and then followed by the formation of TiAl since no enough Al liquid is present near the Ti foil ridge in this work (cf. Ti:Al = 5:1 thickness ratio). Consequently, after all of the liquid Al phase has been consumed into generating TiAl₃, the following high-temperature post-process drives the aluminum atoms continuously to diffuse from the TiAl₃ compound to the residual Ti layers due to the differential concentration of the Al element between TiAl₃ compound and residual Ti layers to form TiAl₂, TiAl and Ti₃Al from the TiAl₃ layer to residual Ti layer [34, 35]. Figure 6b shows the X-ray diffraction analysis of the hybrid composite.

Figure 7a presents the interfacial morphology of one SiC fiber and its surrounding Ti matrix. The SiC fiber is intact with the protection of C coating, which could preserve the fiber strength in hybrid composite, while one clear gray layer is formed between the C coating deposited on SiC fiber and titanium matrix. In Fig. 7b, the EDXS line scans were made along the yellow line in the high-magnification image of the reaction zone. The results suggest that a circular joining of TiC is achieved by reaction between the deposited coating of C and the Ti matrix. The total thickness of the reaction zone was about 2 μm, and no clear defects were observed. These results are in good agreement with the reaction products reported in [19, 33]. However, TiC cannot be detected in the XRD patterns due to its low content.

Mechanical properties of the prepared bio-inspired hybrid composite

Table 2 summarizes the experimental and theoretical tensile and flexural strengths of Ti-intermetallic multi-layered/SiC_f-reinforced Ti-matrix, continuous-SiC_f-reinforced Ti-matrix and Ti-intermetallic multi-layered composites. In comparison with the Ti-intermetallic multi-layered composite, the ultimate tensile and the flexural strengths of the hybrid composite were all enhanced due to the addition of continuous-SiC_f-reinforced Ti-matrix part. In detail, the ultimate tensile and flexural strengths of the hybrid composite have increased of 57 and 92 or 112 %, while the elongation is almost similar to the Ti-intermetallic multi-layered composite. Furthermore, the theoretical tensile strength (σ_s) of hybrid composite was calculated according to:

$$\sigma_s = 50 \% \sigma_{\text{Ti-intermetallic}} + 50 \% \sigma_{\text{SiC}_f\text{-reinforced-Ti}}$$

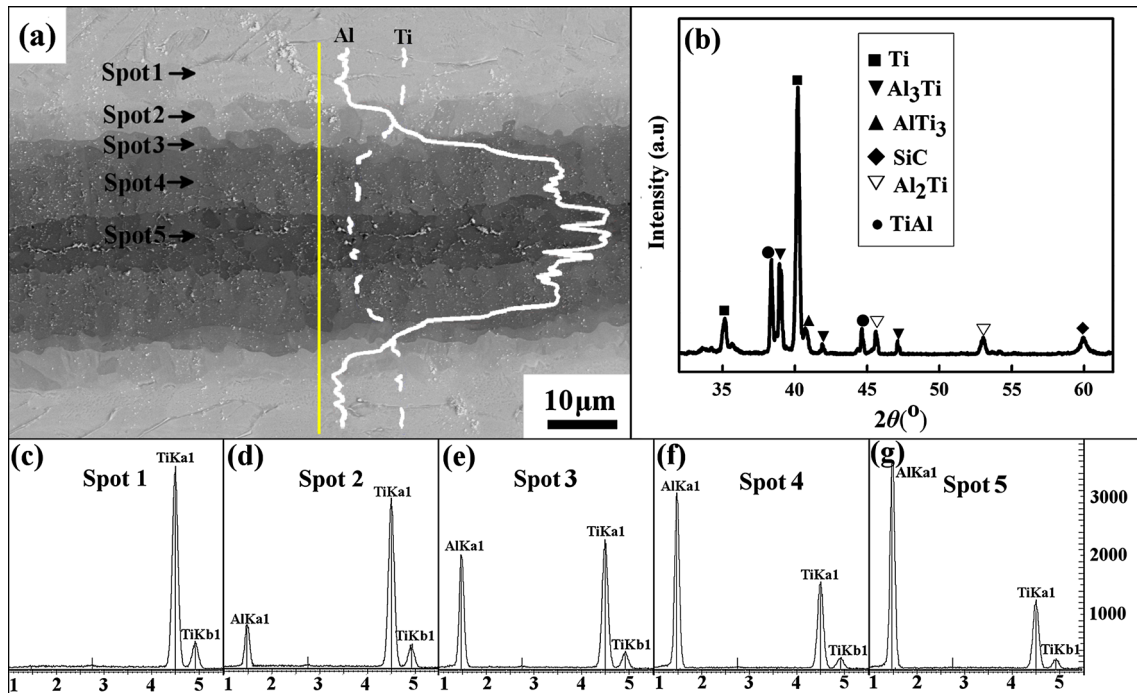


Figure 6 a Typical backscattered electron (BSE) image of the Ti–Al reaction zone, c–g are EDXS quantitative analysis results, b XRD pattern of hybrid composite.

Table 1 EDS point analysis results corresponding to Fig. 6 (at.%)

Point no.	Ti	Al	Phase
Spot 1	99.38	0.62	Ti
Spot 2	72.60	27.40	Ti ₃ Al
Spot 3	49.48	50.52	TiAl
Spot 4	34.19	65.81	TiAl ₂
Spot 5	25.82	74.18	TiAl ₃

The value is about 625 MPa, which is very close to the experimental value (636 ± 40 MPa). This confirms that the tensile strength of synthesized hybrid composite is a combination of two parts. Furthermore, when the hybrid composite was bent from the opposite directions during three-point bending test, different strengths and elongations were obtained. In order to investigate the influence of continuous-SiC_f-reinforced Ti-matrix part and Ti-intermetallic multi-layered part on the hybrid composite, the microstructure and experimental curves after tensile test, three-point bending test, fracture toughness test and drop hammer impact test are separately given and discussed in the next part.

Figure 8a shows the room-temperature tensile stress–strain curves of the synthesized hybrid composite, the continuous-SiC_f-reinforced Ti-matrix

composite and the Ti-intermetallic multi-layered composite. As reported in the literature [36], the stress–strain curve of continuous-SiC_f-reinforced Ti-matrix composite presents the typical fiber’s brittle fracture behavior. After the maximum load, this composite abruptly broke to failure without any ductile deformation region. However, the other two curves have almost the same tensile fracture strain (about 4.2 %). The stress–strain curve of the hybrid composite shows a nearly linear load up to about 636 MPa with a strain of 3.4 % and then suddenly decreased to 561 MPa with a nonlinear elastic region before failure. The latter value is higher than the corresponding one of the Ti-intermetallic multi-layered composite (404 MPa). Therefore, it can be concluded that the behavior during deformation of the synthesized hybrid composite results from the high stiffness of SiC fibers and high strength of Ti–Al multi-layers.

Typical rough fracture surfaces of the three composites are given in Fig. 8b–d. Clear fiber/matrix interface debonding and brittle fiber breakage are observed in Fig. 8b. In contrast, the Ti-matrix alloy shows a typical plastic fracture behavior with nearly equiaxial ductile dimples and tear, as shown in the inset of Fig. 8b. This phenomenon can be explained

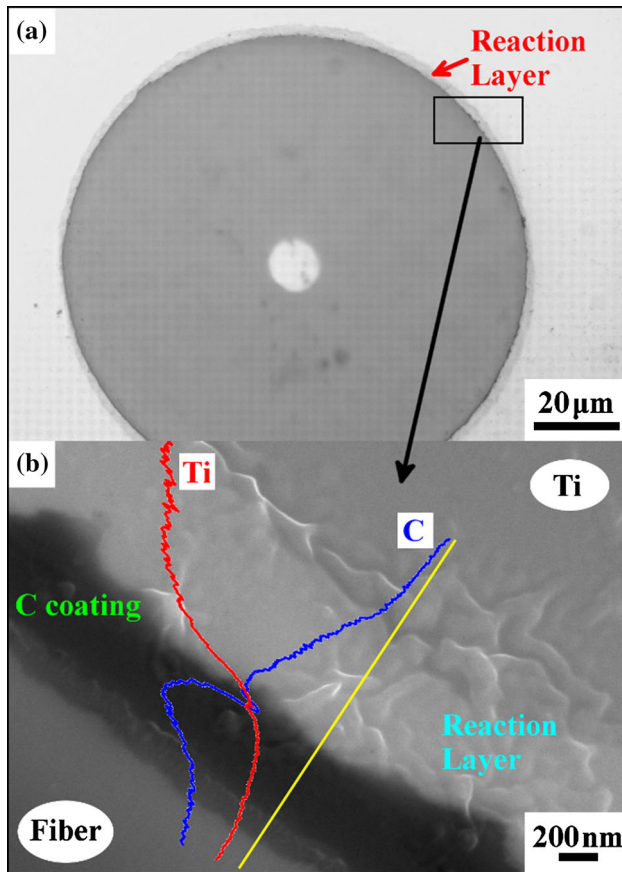


Figure 7 Microstructure and EDXS results of the continuous-SiC_f-reinforced titanium part: **a** interfacial morphology of a SiC fiber and Ti matrix, **b** the interfacial reaction layer between SiC fiber and Ti matrix.

from the difference in elastic modulus between rigid SiC fibers and ductile Ti matrix. Figure 8c shows the typical fractured-layered structure in Ti-intermetallic

multi-layered composite. Similarly, this phenomenon is often found as a main failure mechanism of rigid biological materials, such as abalone shell and clam shell [2, 4]. Concerning about hybrid composite, ductile Ti matrix transferred the load to the rigid SiC fibers during the tensile test. With the increasing load, micro-cracks initiated within rigid SiC fibers and spread into Ti matrix through the generated TiC layers [20, 37]. When the tensile stress reaches the peak point (636 MPa), the rigid SiC fibers are seemingly fractured and result in the debonding of the fiber/matrix interface. Subsequently, the Ti matrix and especially the Ti–Al layers continued to deform under the 561 MPa load. The deformation of Ti layers and Ti–Al intermetallic layers follows the equal strain model based on the lamination theory during the longitudinal tensile test process [38]. Finally, the hybrid composite collapsed at a strain of about 4.2 % in this work. As shown in Fig. 8d, this deformation mechanism resulted in the rugged surface in continuous-SiC_f-reinforced Ti-matrix part and detached layered structure in Ti-intermetallic layers. Furthermore, Fig. 8e, f shows that two parts still kept with each other, which prove that the hybrid composite has successfully been fabricated.

Figure 9a shows four typical load–displacement curves of the un-notched specimens during the three-point bending test. It can be clearly seen that continuous-SiC_f-reinforced Ti-matrix composite and Ti-intermetallic multi-layered composite exhibit typical fiber’s reinforcement effectiveness and Ti–Al layer’s ductile deformation behavior, respectively. Compared to the Ti-intermetallic multi-layered composite, the flexural strength of hybrid composite largely

Table 2 Mechanical properties result of the prepared bio-inspired hybrid composite, Ti-intermetallic multi-layered composite and continuous-SiC_f-reinforced Ti-matrix composite in this research

Material	UTS (MPa)	Elongation (%)	Fracture toughness	Flexural strength (MPa)
Hybrid composite	636 ± 40	4.2 ± 0.5		889 ± 50 Ti-intermetallic stressed in tension 984 ± 50 Continuous-SiC _f stressed in tension
Ti-intermetallic multi-layered composite	404 ± 30	4.3 ± 0.5	34.7 ± 1.2 MPa m ^{1/2}	462 ± 30
Continuous-SiC _f -reinforced Ti-matrix composite	876 ± 50	3.0 ± 0.2	24.8 ± 0.1 MPa m ^{1/2}	1224 ± 30

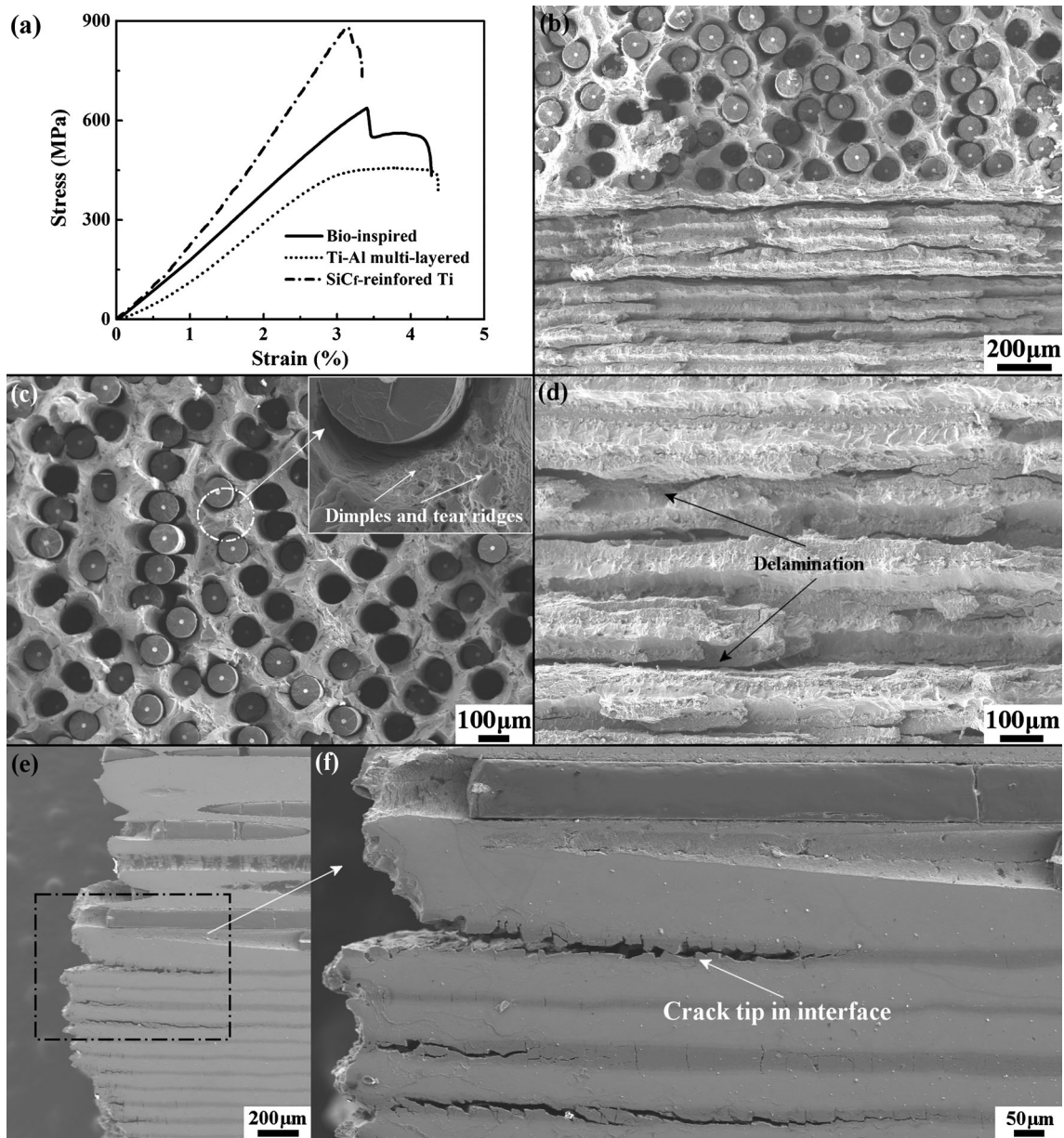


Figure 8 a Stress–strain curves of prepared bio-inspired hybrid composite (solid line), Ti-intermetallic multi-layered composite (dotted line) and continuous-SiC_F-reinforced Ti-matrix composite (dash-dotted line); b–d fractographs of continuous-SiC_F-reinforced

Ti composite, Ti–Al multi-layered composite and hybrid composite after tensile loading. e, f crack tip propagation in interface between two parts in hybrid composite.

increased due to the addition of continuous-SiC_F-reinforced Ti-matrix part. As the deformation of bio-inspired hybrid composite is a combination of these two parts, it is expected that the hybrid composite exhibits different responses under different load directions. Compared to the Ti-intermetallic multi-layered part stressed in tension (named Layer in tension), the hybrid composite exhibited higher

damage tolerance coupled with a longer deformed platform when continuous-SiC_F-reinforced Ti-matrix part was stressed in tension. (This one is also similar to the predator’s bite [39], named Fiber in tension.) For understanding this difference, the surface morphologies of hybrid composite after three-point bending tests on the two different sides are shown in Fig. 9b, c. When Ti-intermetallic multi-layered part

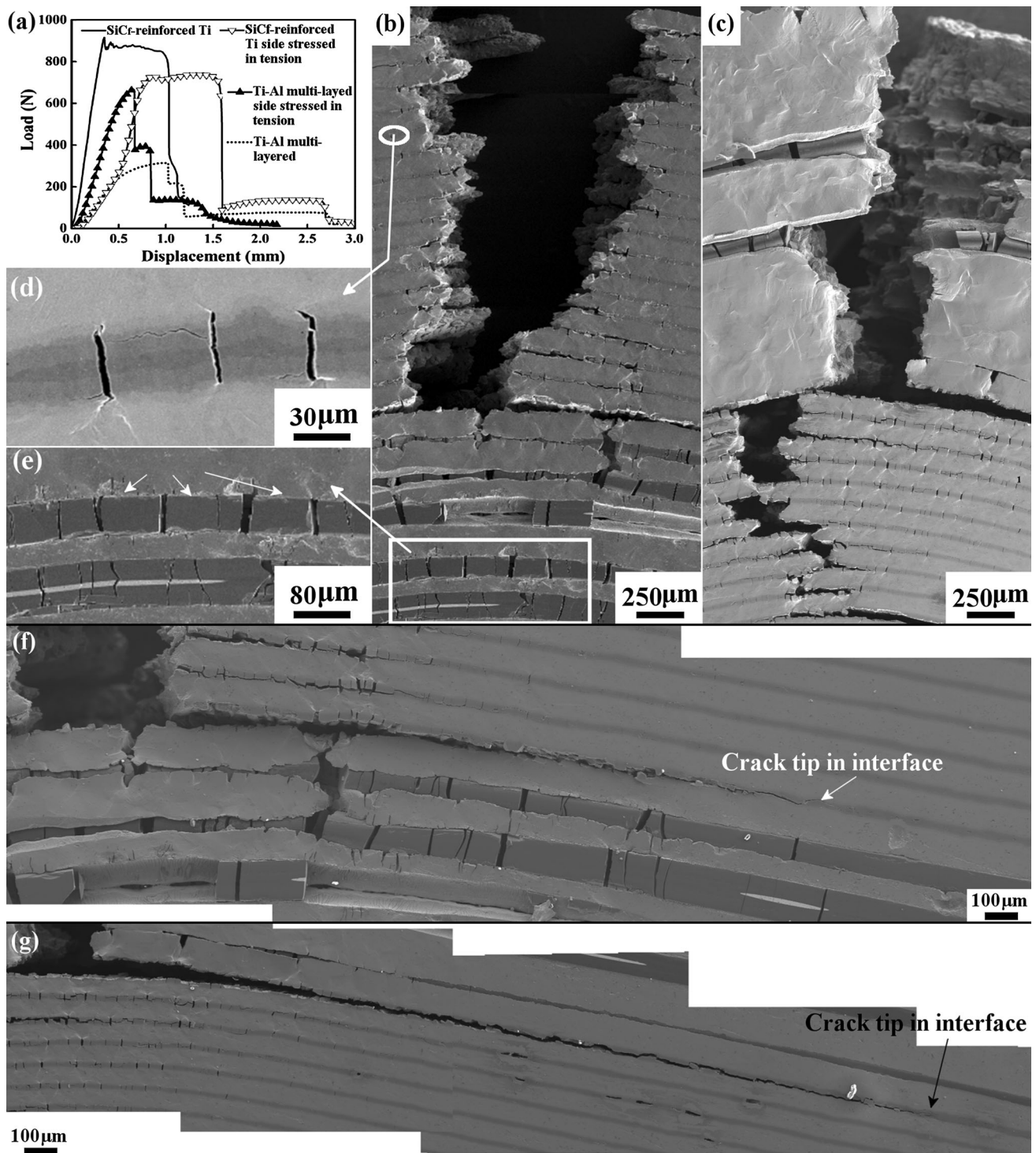


Figure 9 a Load–displacement curves of prepared composites in three-point bending test. For bio-inspired hybrid composite, continuous-SiC_f-reinforced Ti-matrix part stressed in tension (*solid line* interspersed with *hollowed triangular symbols*) and Ti–Al multi-layered part stressed in tension (*solid line* interspersed with *black solid triangular symbols*), Ti-intermetallic multi-layered

composite (*dotted line*), continuous-SiC_f-reinforced Ti-matrix composite (*solid line*), **b**, **c** morphology and propagation of the main cracks of the prepared bio-inspired hybrid composite, **d**, **e** high magnitude morphologies of the micro-cracks within the Ti-intermetallic multi-layered part and fractured fibers, **f**, **g** crack propagation in interface between two parts.

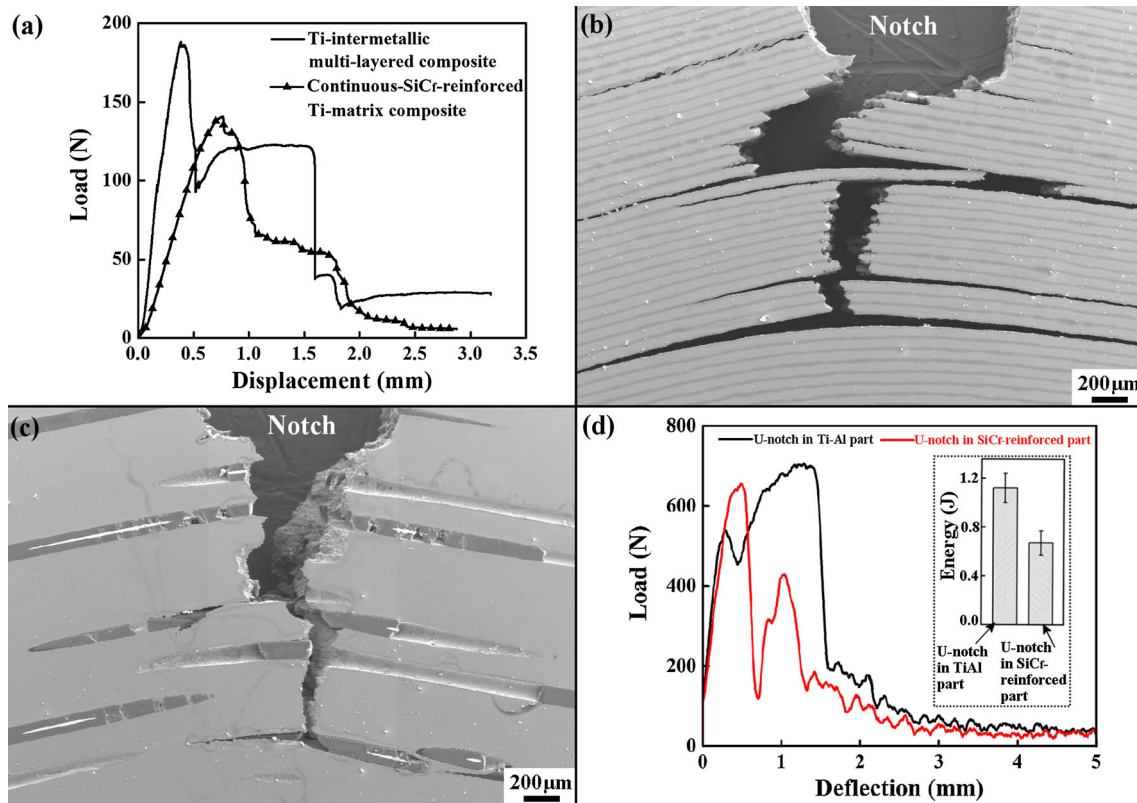


Figure 10 a–c Load–displacement curves, morphology and propagation of the main cracks in the notched TiAl multi-layered composite and SiC_f-reinforced Ti composite, d load–displacement

curves were recorded on notched hybrid composite by oscilloscope in drop hammer test. The *inset* represents the absorbed energy of drop hammer tests on notched hybrid composite.

was stressed in tension, the crack propagation firstly presents a step structure within the Ti-intermetallic multi-layers [40]. Besides, multiple micro-cracks are identified within the Ti–Al intermetallic layers, as illustrated in Fig. 9d. When continuous-SiC_f-reinforced Ti-matrix part was stressed in tension, the difference in elastic modulus and in Poisson ratio between SiC fibers and Ti matrix triggers the disparity in stress distribution, which resulted in a higher tensile stress on the rigid SiC fibers and favored the rupture of the fibers in a brittle pattern. Fortunately, further propagation of the micro-cracks could be suppressed by the ductile Ti matrix. Furthermore, the broken pieces of SiC fibers still kept strengthen Ti matrix due to the formed TiC layer between Ti and SiC fiber (indicated by white arrows in Fig. 9e). Herein, due to the reinforced effect of the SiC fibers and ductile ability of Ti, the hybrid composite shows a higher damage tolerance when continuous-SiC_f-reinforced Ti-matrix part was stressed in tension. Furthermore, Fig. 9f, g reveals that the two

parts still kept in touch with each other after the specimen failure.

Figure 10a presents the curves of load–displacement obtained from the notched Ti-intermetallic multi-layered composite and continuous-SiC_f-reinforced Ti-matrix composite, respectively. Like the un-notched specimen, Fig. 10b shows that notched Ti-intermetallic multi-layered composite still presents one step-like response. This should be attributed to the crack deflection ability and damage tolerance of the multi-layered structure. Concerning about continuous-SiC_f-reinforced Ti-matrix composite, in contrast to the un-notched sample, no plateau was found after the yielding point. The declined curve after the yielding points indicates that notched continuous-SiC_f-reinforced Ti-matrix composite was more sensitive to the crack propagation than the un-notched one. This was also confirmed in Fig. 10c that the ductile deformation in Ti matrix can be hardly found in the fracture morphology.

As the ratio between two parts is 1 in the hybrid composite, the standard fracture toughness test

cannot be performed regularly. Herein, we adopted the drop hammer impact test to evaluate the responses of the hybrid composite from two opposite directions, as shown in Figs. 4d and 10d. From load–displacement curves, the curve with U notch in Ti-intermetallic multi-layered side (this one is also similar to the predator's bite) is characterized with one peak and a long plateau before failure. However, for the curve obtained with U notch in continuous-SiC_F-reinforced Ti-matrix side, no plateau was found. It was marked with one peak resulted from the fracture of continuous-SiC_F-reinforced Ti-matrix part and the subsequent peaks resulted from the multi-layered structure in Ti-intermetallic multi-layered side [41]. Additionally, the inset histogram in Fig. 10d shows the absorbed energy of drop hammer impact test in two cases. These differences strongly suggest that fracture resistance of hybrid is strongly enhanced due to the protection of Ti-intermetallic multi-layered part to the underneath continuous-SiC_F-reinforced Ti-matrix part. This behavior is very similar to the fracture behavior of outer layer of turtle shell. The multi-layered keratin could deflect the crack propagation with a step structure, and the carbonaceous fibers could reinforce the dorsal cortex by fibers pulling out [6].

Conclusions

1. Bio-inspired hybrid Ti-intermetallic multi-layered/SiC_F-reinforced Ti-matrix composites were successfully fabricated by high-temperature reaction sintering in vacuum atmosphere using pure titanium foils, pure aluminum foils and continuous SiC ceramic fibers.
2. Under a vacuum hot-pressing sintering procedure, the initially selected components were firmly bonded to each other by diffusion and reaction zone. In the Ti-intermetallic part, intermetallic phases such as Ti₃Al, TiAl, TiAl₂ and TiAl₃ were formed. Additionally, TiC compound was produced through the reaction between Ti matrix and deposited C coating on SiC fibers.
3. Along the longitudinal direction of the SiC fibers, the tensile and the flexural strengths of the hybrid composite were 636 ± 40 and 889 ± 50 MPa (Ti-intermetallic multi-layered part stressed in tension) or 984 ± 50 MPa (continuous-SiC_F-reinforced Ti-matrix part stressed in tension),

respectively. These values were much higher than those obtained from Ti-intermetallic multi-layers composite, corresponding to 404 ± 30 and 462 ± 30 MPa. But they were lower than those obtained from SiC fiber-reinforced Ti matrix, corresponding to 876 ± 90 and 1224 ± 30 MPa, respectively. Furthermore, the hybrid and the Ti-intermetallic multi-layered composites have almost the same elongation (about 4.2 %), which is much higher than that of continuous-SiC_F-reinforced Ti-matrix composites (about 3 %).

4. Ti-intermetallic multi-layered composite shows higher fracture toughness value (34.7 ± 1.2 MPa m^{1/2}) than continuous-SiC_F-reinforced Ti-matrix composite (24.8 ± 0.1 MPa m^{1/2}). In drop hammer impact test, the hybrid composite showed better crack resistance and higher absorb energy when the U notch was in Ti-intermetallic multi-layered side, other than in continuous-SiC_F-reinforced Ti-matrix side.
5. According to the morphology observation, it reveals that the hybrid composite owns the crack deflection ability of Ti-intermetallic multi-layered structure and strengthens the effect of continuous SiC fibers. In particular, when the hybrid composite was impacted with the U notch in Ti-intermetallic multi-layered side, Ti-intermetallic multi-layered structure could deflect the crack propagation and protect the underneath SiC_F-reinforced Ti matrix.

Acknowledgements

This work was financially supported by Innovation Platform for Thought Process Modeling and Simulation of Advanced Materials Processing Technologies Project of China (2012ZX04012-011) and supported by the class General Financial Grant from the China Postdoctoral Science Foundation (2015M580093).

References

- [1] Mayer G (2005) Rigid biological systems as models for synthetic composites. *Science* 310:1144. doi:10.1126/science.1116994
- [2] Meyers MA, Chen P-Y, Lin AY-M, Seki Y (2008) Biological materials: structure and mechanical properties. *Prog Mater Sci* 53:1. doi:10.1016/j.pmatsci.2007.05.002

- [3] Chen P-Y, McKittrick J, Meyers MA (2012) Biological materials: functional adaptations and bioinspired designs. *Prog Mater Sci* 57:1492. doi:10.1016/j.pmatsci.2012.03.001
- [4] Chen Q, Pugno NM (2013) Bio-mimetic mechanisms of natural hierarchical materials: a review. *J Mech Behav Biomed Mater* 19:3. doi:10.1016/j.jmbbm.2012.10.012
- [5] Rhee H, Horstemeyer MF, Hwang Y, Lim H, El Kadiri H, Trim W (2009) A study on the structure and mechanical behavior of the *Terrapene carolina* carapace: a pathway to design bio-inspired synthetic composites. *Mater Sci Eng, C* 29:2333. doi:10.1016/j.msec.2009.06.002
- [6] Balani K, Patel RR, Keshri AK, Lahiri D, Agarwal A (2011) Multi-scale hierarchy of *Chelydra serpentina*: microstructure and mechanical properties of turtle shell. *J Mech Behav Biomed Mater* 4:1440. doi:10.1016/j.jmbbm.2011.05.014
- [7] Damiens R, Rhee H, Hwang Y et al (2012) Compressive behavior of a turtle's shell: experiment, modeling, and simulation. *J Mech Behav Biomed Mater* 6:106. doi:10.1016/j.jmbbm.2011.10.011
- [8] Zhang W, Wu C, Zhang C, Chen Z (2012) Numerical study of the mechanical response of turtle shell. *J Bionic Eng* 9:330. doi:10.1016/s1672-6529(11)60129-7
- [9] Achrai B, Wagner HD (2013) Micro-structure and mechanical properties of the turtle carapace as a biological composite shield. *Acta Biomater* 9:5890. doi:10.1016/j.actbio.2012.12.023
- [10] Achrai B, Bar-On B, Wagner HD (2014) Bending mechanics of the red-eared slider turtle carapace. *J Mech Behav Biomed Mater* 30:223. doi:10.1016/j.jmbbm.2013.09.009
- [11] Rawers JC, Hansen JS, Alman DE, Hawk JA (1994) Formation of sheet-metal intermetallic composites by self-propagating high-temperature reactions. *J Mater Sci Lett* 13:1357. doi:10.1007/Bf00624495
- [12] Alman DE, Rawers JC, Hawk JA (1995) Intermetallic sheets synthesized from elemental Ti, Al, and Nb foils. *Metall Mater Trans A* 26A:589. doi:10.1007/BF02669433
- [13] Rawers JC, Maupin HE (1993) Metal–intermetallic composites formed by reaction-sintering metal foils. *J Mater Sci Lett* 12:637. doi:10.1007/Bf00465576
- [14] Harach DJ, Vecchio KS (2001) Microstructure evolution in metal–intermetallic laminate (MIL) composites synthesized by reactive foil sintering in air. *Metall Mater Trans A* 32A:1493. doi:10.1007/s11661-001-0237-0
- [15] Sheng LY, Yang F, Xi TF, Lai C, Ye HQ (2011) Influence of heat treatment on interface of Cu/Al bimetal composite fabricated by cold rolling. *Compos B Eng* 42:1468. doi:10.1016/j.compositesb.2011.04.045
- [16] Zhong Y, Chen H, Hu W, Gottstein G (2007) Fiber damage and high temperature tensile properties of Al₂O₃ fiber reinforced NiAl-matrix composites with and without hBN-interlayer. *Mater Sci Eng A* 464:241. doi:10.1016/j.msea.2007.02.072
- [17] Zhang G, Bingchao L, Zhang J, Cai W (2012) The strain amplitude-controlled cyclic fatigue behavior of Al₂O₃ fiber reinforced Al–Si alloy composite at elevated temperatures. *Prog Nat Sci Mater Int* 22:153. doi:10.1016/j.pnsc.2012.03.009
- [18] Guo SQ, Kagawa Y (1997) Characterization of interface sliding damage in SiC fiber-reinforced Ti-15-3 matrix composite by cyclic fatigue. *Acta Mater* 45:2257. doi:10.1016/S1359-6454(96)00356-4
- [19] Fu YC, Shi NL, Zhang DZ, Yang R (2006) Effect of C coating on the interfacial microstructure and properties of SiC fiber-reinforced Ti matrix composites. *Mater Sci Eng A* 426:278. doi:10.1016/j.msea.2006.04.029
- [20] Feng GH, Yang YQ, Luo X, Li J, Huang B, Chen Y (2015) Fatigue properties and fracture analysis of a SiC fiber-reinforced titanium matrix composite. *Compos B Eng* 68:336. doi:10.1016/j.compositesb.2014.09.005
- [21] Peng LM, Wang JH, Li H, Zhao JH, He LH (2005) Synthesis and microstructural characterization of Ti–Al₃Ti metal–intermetallic laminate (MIL) composites. *Scripta Mater* 52:243. doi:10.1016/j.scriptamat.2004.09.010
- [22] Oh J, Lee WC, Pyo SG, Park W, Lee S, Kim NJ (2002) Microstructural analysis of multilayered titanium aluminide sheets fabricated by hot rolling and heat treatment. *Metall Mater Trans A* 33:3649. doi:10.1007/s11661-002-0239-6
- [23] Bataev IA, Bataev AA, Mali VI, Pavliukova DV (2012) Structural and mechanical properties of metallic–intermetallic laminate composites produced by explosive welding and annealing. *Mater Des* 35:225. doi:10.1016/j.matdes.2011.09.030
- [24] Sun Y, Vajpai SK, Ameyama K, Ma C (2014) Fabrication of multilayered Ti–Al intermetallics by spark plasma sintering. *J Alloy Compd* 585:734. doi:10.1016/j.jallcom.2013.09.215
- [25] Rawers JC, Alman DE (1995) Fracture characteristics of metal/intermetallic laminar composites produced by reaction sintering and hot-pressing. *Compos Sci Technol* 54:379. doi:10.1016/0266-3538(95)00072-0
- [26] Rohatgi A, Harach DJ, Vecchio KS, Harvey KP (2003) Resistance-curve and fracture behavior of Ti–Al₃Ti metallic–intermetallic laminate (MIL) composites. *Acta Mater* 51:2933. doi:10.1016/s1359-6454(03)00108-3
- [27] Naseem K, Yang Y, Luo X, Huang B, Feng G (2011) SEM in situ study on the mechanical behaviour of SiC_f/Ti composite subjected to axial tensile load. *Mater Sci Eng A* 528:4507. doi:10.1016/j.msea.2011.02.064
- [28] Luo X, Yang Y, Sun Q, Yu Y, Huang B, Chen Y (2012) Effect of Cu/Mo duplex coating on the interface and property of SiC_f/Ti6Al4 V composite. *Mater Sci Eng A* 535:6. doi:10.1016/j.msea.2011.12.029

- [29] Guo SQ, Kagawa Y, Bobet JL, Masuda C (1996) Fatigue damage evolution in SiC fiber-reinforced Ti-15-3 alloy matrix composite. *Mater Sci Eng* 220:57. doi:[10.1016/S0921-5093\(96\)10438-X](https://doi.org/10.1016/S0921-5093(96)10438-X)
- [30] Froes FH, Suryanarayana C, Eliezer D (1992) Synthesis, properties and applications of titanium aluminides. *J Mater Sci* 27:5113. doi:[10.1007/Bf00553381](https://doi.org/10.1007/Bf00553381)
- [31] Lou JH, Yang YQ, Sun Q, Li J, Luo X (2011) Study on longitudinal tensile properties of SiC_f/Ti-6Al-4 V composites with different interfacial shear strength. *Mater Sci Eng A* 529:88. doi:[10.1016/j.msea.2011.09.002](https://doi.org/10.1016/j.msea.2011.09.002)
- [32] Sujata M, Bhargava S, Sangal S (1997) On the formation of TiAl₃ during reaction between solid Ti and liquid Al. *J Mater Sci Lett* 16:1175. doi:[10.1007/Bf02765402](https://doi.org/10.1007/Bf02765402)
- [33] Xu L, Cui YY, Hao YL, Yang R (2006) Growth of intermetallic layer in multi-laminated Ti/Al diffusion couples. *Mater Sci Eng A* 435–436:638. doi:[10.1016/j.msea.2006.07.077](https://doi.org/10.1016/j.msea.2006.07.077)
- [34] van Loo FJJ, Rieck GD (1973) Diffusion in the titanium–aluminium system—I. Interdiffusion between solid Al and Ti or Ti–Al alloys. *Acta Metall* 21:61. doi:[10.1016/0001-6160\(73\)90220-4](https://doi.org/10.1016/0001-6160(73)90220-4)
- [35] Van Loo FJJ (1971) Diffusion in the titanium-aluminium system—I. Interdiffusion between solid Al and Ti or Ti–Al alloys. *Eindh Tech Hogesch Eindh*. doi:[10.6100/ir36207](https://doi.org/10.6100/ir36207)
- [36] Jeng SM et al (1992) Mechanical behaviour of SiC fibre-reinforced titanium titanium aluminide hybrid composites. *J Mater Sci* 27:5357. doi:[10.1007/bf00553419](https://doi.org/10.1007/bf00553419)
- [37] Gundel DB, Miracle DB (1998) Transverse tensile behavior of SiC-fiber/Ti-6Al-4 V composites—1. Experimental results. *Compos Sci Technol* 58:1571. doi:[10.1016/S0266-3538\(97\)00217-0](https://doi.org/10.1016/S0266-3538(97)00217-0)
- [38] Jeong C, Oya T, Yanagimoto J (2013) Analysis of fracture behavior and stress–strain distribution of martensite/austenite multilayered metallic sheet. *J Mater Process Technol* 213:614. doi:[10.1016/j.jmatprotec.2012.10.017](https://doi.org/10.1016/j.jmatprotec.2012.10.017)
- [39] Heithaus MR, Wirsing AJ, Thomson JA, Burkholder DA (2008) A review of lethal and non-lethal effects of predators on adult marine turtles. *J Exp Mar Biol Ecol* 356(1–2):43–51
- [40] Sun Y, Chen J, Ma F, Ameyama K, Xiao W, Ma C (2015) Tensile and flexural properties of multilayered metal/intermetallics composites. *Mater Charact* 102:165. doi:[10.1016/j.matchar.2015.02.018](https://doi.org/10.1016/j.matchar.2015.02.018)
- [41] Cao Y, Guo C, Zhu S, Wei N, Javed RA, Jiang F (2015) Fracture behavior of Ti/Al₃Ti metal–intermetallic laminate (MIL) composite under dynamic loading. *Mater Sci Eng A* 637:235–242